*Machine Copy for Proofreading, Vol. x, y–z, 2012*

# THE UNFOLDING OF BANDGAP DIAGRAMS OF HEXAGONAL PHOTONIC CRYSTALS COMPUTED WITH FDTD

**B. Salski***

Institute of Radioelectronics, Warsaw University of Technology, 15/19 Nowowiejska, Warsaw 00-665, Poland

**Abstract**—The application of the finite-difference time-domain method with rectangular periodic boundary conditions to the analysis of a hexagonal photonic crystal results in a folded bandgap diagram. The aim of this paper is to introduce a new unfolding method, which allows unambiguously determining the position of the modes in a wave-vector space by taking the advantage of the fast Fourier transform of modal field distributions. Unlike alternative solutions, it does not require any modifications of the FDTD method and is based solely on the post-processing of the simulation results. The proposed method can be applied to any non-rectangular lattice types, such as hexagonal, face-centered cubic or body-centered cubic.

## 1. INTRODUCTION

Photonic crystals (PhCs) have been extensively studied for over two decades and still bring a lot of attention of both scientific and industrial communities [1]. Simultaneously, it has prompted a significant advance of numerical methods applicable to the modeling and design of such optical devices, consisting of the photonic crystals, as planar waveguides [2], directional couplers [3], micro-structured fibers [4], filters [5], lasers [6]. In principle, there are two types of electromagnetic problems that are of interest when considering photonic crystals, namely, eigenvalue and deterministic problems [7]. The former one refers to the spectral properties of the PhC itself, while the latter one concerns the scenarios with external electromagnetic sources.

In this paper, the attention is focused on the eigenvalue problems only, usually given in the form of a photonic bandgap diagram

*Received 13 August 2012.*

* Corresponding author: Bartlomiej Salski (bsalski@ire.pw.edu.pl).

(PBG) showing the dependence of allowed modal frequencies on a wavenumber $\omega(k)$ spanned over the contour of an irreducible Brillouin zone [1]. In most cases, the advantage of the Floquet theorem [8] is taken, which allows reducing a computational model to a single period of an investigated lattice. The implementation of that approach can be found in such methods as plane wave expansion (PWE) [9, 10], finite-element method (FEM) [11], finite-difference frequency-domain (FDFD) method [12] or finite-difference time-domain (FDTD) method [13]. PWE is computationally efficient when dealing with relatively simple structures but requires special approximate averaging techniques to account for non-rectangular geometries [10]. FEM is one of the most common frequency-domain techniques, which allows the modeling of arbitrarily-shaped geometries. There is also FDFD, which solves Maxwell curl equations in a frequency-domain by matrix inversion. Eventually, FDTD is a versatile time-domain technique, naturally adapted to a wideband analysis of electromagnetic scenarios. Moreover, if a simulation tool is equipped with a conformal FDTD meshing technique [14, 15], non-rectangular geometries can be easily taken into account on a rectangular FDTD grid, without any increase of computational effort of the simulation. The aforementioned features are some of the reasons that FDTD is frequently applied to the computation of PBG diagrams of more complicated geometries, such as PhC membranes [16] or quantum cascade lasers [17]. It should be also emphasized that FDTD is very competitive when the scenario is electrically large, since the computational cost of the method increases not that large as for other full-wave numerical methods [13].

There are a few extensions of the FDTD algorithm accounting for the spatial periodicity, such as CL-FDTD [18] or sin/cos technique [19]. In those methods, periodic boundary conditions (PBCs), derived from the Floquet theorem, are imposed on the lateral sides of the model truncated to a unit rectangular cell of the lattice. However, since FDTD is based on rectangular discretization of space, PBCs of that kind are applicable only along the Cartesian axes and cannot be straightforwardly applied at an oblique direction. It implies that the modeling of non-rectangular lattice geometries, like hexagonal one, becomes an issue for FDTD. Consequently, as it will be shown in this paper, a rectangular unit FDTD cell representing a hexagonal lattice generates a folded bandgap diagram, thus, leading to ambiguity of the solution. However, this is not specific to FDTD only, but to any other method working with rectangular mesh.

In the literature, several techniques are proposed to overcome that limitation. The first method is based on a non-orthogonal FDTD

mesh formulation, enabling oblique periodic boundary conditions to be imposed [20, 21]. However, most of the available FDTD solvers do not allow for such unusual mesh generation, mainly due to vague stability criteria for irregular FDTD mesh [13]. Moreover, the transformation of both Maxwell equations and a coordinate system is required. In the second approach, an approximate rectangular unit lattice cell is created from the hexagonal one by rearranging the geometry of the lattice [22, 23]. However, no formal proof of concept is given for that method, so it cannot be applied automatically without special caution. The third method applies oblique PBCs truncating the unit lattice cell composed of rectangular FDTD cells at oblique edges [24]. The method is potentially unstable, so the original FDTD algorithm has to be modified to account for that. For several users this is not achievable as they are using commercial FDTD solvers.

This paper presents a simple, robust and efficient algorithm for the generation of the unfolded PBG diagrams, which is applicable with a classic FDTD algorithm supplemented with rectangular PBCs. The investigation is concentrated on hexagonal PhCs, although the method can be easily extended to any other non-rectangular lattice types. In Section 2, the folding of a bandgap diagram of a hexagonal lattice, due to a rectangular shape of a computational model, is addressed. Subsequently, the unfolding procedure is introduced and validated in Section 3.

## 2. FOLDED BANDS

Consider an example of a two-dimensional (2D) hexagonal photonic crystal as shown in Figure 1(a). The structure is made of air-gaps processed in a dielectric substrate ($\varepsilon_r = 13$) [1]. A dashed line indicates the boundaries of an FDTD model of a rectangular unit cell of the considered hexagonal lattice, the mesh of which is shown in Figure 1(b). Such a simple example has been deliberately chosen to concentrate on the unfolding procedure only and avoid extensive studies on the structure itself and the performance of electromagnetic simulations.

Figure 2 shows a reciprocal hexagonal lattice (blue color in online version) of the photonic crystal shown in Figure 1(a). Additional black marks indicated in the Figure 2 will be explained in Section 3. Critical points of the reciprocal lattice can be given as follows:

$$\vec{k}_\Gamma = 0 \tag{1}$$

$$\vec{k}_M = \frac{2\pi}{\sqrt{3}a}\hat{i}_y \tag{2}$$

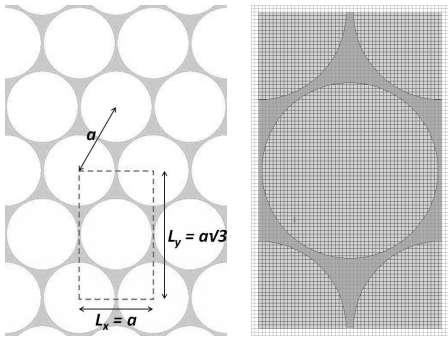


**Figure 1.** (a) A 2D hexagonal photonic crystal made of air gaps hollowed in a dielectric substrate ($\varepsilon_r = 13$) [1] and (b) an FDTD mesh of a unit rectangular cell.

$$\vec{k}_K = \frac{4\pi}{3a}\hat{i}_x \tag{3}$$

Since the FDTD model of the hexagonal lattice is rectangular, as shown in Figure 1(b), the corresponding reciprocal lattice is rectangular as well and has the critical points, depicted with green in Figure 2, which are given as follows:

$$\vec{k}_{X1} = \frac{\pi}{a}\hat{i}_x = \frac{3}{4}\vec{k}_K \tag{4}$$

$$\vec{k}_{X2} = \frac{\pi}{\sqrt{3}a}\hat{i}_y = \frac{1}{2}\vec{k}_M \tag{5}$$

It can be noticed from (4) and (5) that a horizontal (vertical) length of the rectangular unit cell is 3/4 (1/2) of its hexagonal counterpart. As it can be seen in Figure 2, every second cell of the rectangular reciprocal lattice falls, both horizontally and vertically, in the same position with respect to the hexagonal lattice. Consequently, since the reciprocal rectangular lattice of the FDTD model overlaps with the original hexagonal one, the bands are folding. For instance, imposing the phase shift $(\psi_x, \psi_y) = (2\pi/3, 0)$ along the horizontal $\Gamma$-$K$ contour, the propagation of $K$ modes is also allowed at the following harmonics: $(\psi_x, \psi_y) = [2\pi/3+2m\pi, 2(n+1)\pi]$ and $(\psi_x, \psi_y) = [2\pi/3 + 2(m+1)\pi, 2n\pi]$, where $m$ and $n$ are integer.

However, it should be emphasized that, due to the folding of both reciprocal lattices, scanning of the rectangular one along $\Gamma$-$X_1$ (red curve in online version) and $\Gamma$-$X_2$ (black curve in online version) contours, completely cover the whole Brillouin zone of the hexagonal

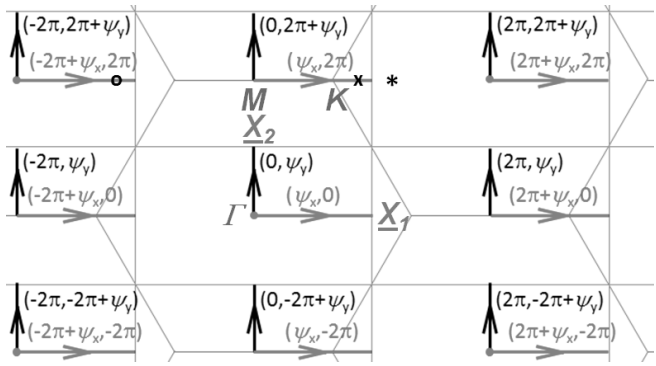


**Figure 2.** A reciprocal lattice of a hexagonal photonic crystal (blue color in online version) as shown in Figure 1(a) and a reciprocal lattice of the corresponding rectangular unit FDTD cell (green color in online version) as shown in Figure 1(b).

lattice. For instance, according to (4), the Γ-$X_1$ contour covers only 3/4 of the Γ-$K$ one, but due to the bands folding, the remaining part of the Γ-$K$ contour is covered by the neighboring rectangular harmonic, that is by the end of the $(-2\pi+\psi_x, 0)$ contour (see Figure 2). Similarly, the Γ-$X_2$ contour covers only 1/2 of the Γ-$M$ one, but the rectangular harmonic at the $(0, -2\pi + \psi_y)$ contour covers the rest of the Γ-$M$ contour.

Ambiguity introduced by such folding is one of the main challenges for the FDTD method, when applied to the modeling of hexagonal photonic crystals. For that reason, an efficient and robust unfolding procedure, which is supposed to overcome the addressed issue, is proposed in the next Section.

## 3. UNFOLDING THE BANDS

A computational model of the photonic crystal structure, the FDTD mesh of which is shown in Figure 1(b), consists of a single layer of FDTD cells placed between electric (magnetic) boundary conditions, thus, enabling the propagation of TM (TE) modes with respect to the $z$-axis. Thus, the TM (TE) mode consists of $H_x$, $H_y$, $E_z$ ($E_x$, $E_y$, $H_z$) field components. The model with the lattice constant set to $a = 1\,\mu$m consists of $50 \times 87$ FDTD cells, the size of which is 20 nm, while an FDTD time step is set to $dt = 33.3as$ to satisfy an FDTD stability criterion. Next, periodic boundary conditions with $\psi_x$ and $\psi_y$ Floquet phase shifts per period are imposed at the lateral sides of the model [8].

The model is excited with a point source, indicated with a red dot in Figure 1(b) driven with the Kronecker delta to evenly cover the whole spectrum of our interest. The computation is executed using a CL-FDTD method dedicated to the analysis of periodic electromagnetic problems [18, 25]. A single CL-FDTD simulation, for a given set of phase shifts $(\psi_x, \psi_y)$, runs with the speed of 7750 FDTD iterations per second and takes in total 6 seconds on an Intel Core i7 CPU 950 platform. It indicates that the solution converges after ca. 1.55 ps.

Figure 3 depicts a flow chart of a photonic bandgap diagram calculation with the unfolding procedure included. For each set of chosen phase shifts $(\psi_x, \psi_y)$ along $\Gamma$-$X_1$ and $\Gamma$-$X_2$ contours indicated in Figure 2, an FDTD simulation is executed to collect resonant frequencies indicating the modes satisfying the imposed phase shifts per period [7, 26]. The example of the spectrum of an electric current of a TM mode for $(\psi_x, \psi_y) = (4/9, 0)2\pi$ injected by the point source is shown in Figure 4. Once the resonant frequencies are determined, the FDTD simulation is run once again with the same settings. This time, however, Fourier transforms are executed to obtain the modal field distributions at the previously detected resonant frequencies. The alternative to the Fourier transform is to run several FDTD simulations with a sinusoidal excitation to store relevant field

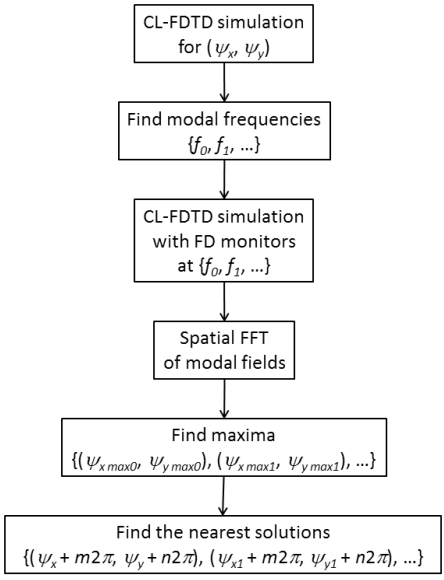


**Figure 3.** A flow chart of a photonic bandgap diagram calculation with the unfolding procedure.

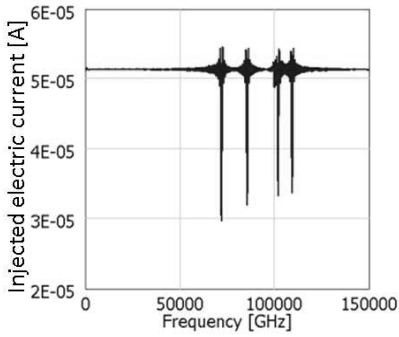


**Figure 4.** The spectrum of an electric current injected by a TM-polarized point source ($E_z$ component) into the structure shown in Figure 1 for $(\psi_x, \psi_y) = (4/9, 0)2\pi$.

distributions. However, the option with Fourier transforms requires only one additional simulation per each set of Floquet phase shifts per period $(\psi_x, \psi_y)$, thus, reducing computational effort to the necessary minimum.

Figures 5(a) and 5(b) show a real part of a Fourier transform of an electric field amplitude $E_z$ computed at 102100 GHz and 109700 GHz, respectively, as taken from Figure 4. Those field distributions are computed for a $1 \times 1$ array of the structure shown in Figure 1(b) and it can be observed that the modes are similar to each other. In the next step of the unfolding procedure, a spatial fast Fourier transform (FFT) of those field distributions is performed to determine the position of dominant spatial harmonics. Figures 5(c) and 5(d) show the corresponding spatial FFTs calculated at both frequencies, respectively. It can be noticed that the dominant modes lay relatively close to each other both centred at $\psi_x = 0$ rad, which is in contradiction with the imposed phase shift of $\psi_x = 4/9$ rad.

In such a case, it is recommended to enlarge the model to a few unit cells in order to increase the resolution of the spatial FFT. For that purpose, Figures 6(a) and 6(b) show a real part of a complex electric field amplitude $E_z$ computed with FDTD at 102100 GHz and 109700 GHz, respectively, in a $4 \times 4$ array of the structure shown in Figure 1. Due to a 4 times larger size of the model, when compared with the previously considered $1 \times 1$ array, Floquet phase shifts have been rescaled accordingly to $(\psi_x, \psi_y) = (16/9, 0)2\pi$. The corresponding spatial FFTs shown in Figures 6(b) and 6(c) indicate the modes to be centred at $(\psi_x, \psi_y) = (0.4237, 1.0722)2\pi$ and $(0.5235, 0.9864)2\pi$, respectively. Comparing those numbers with the

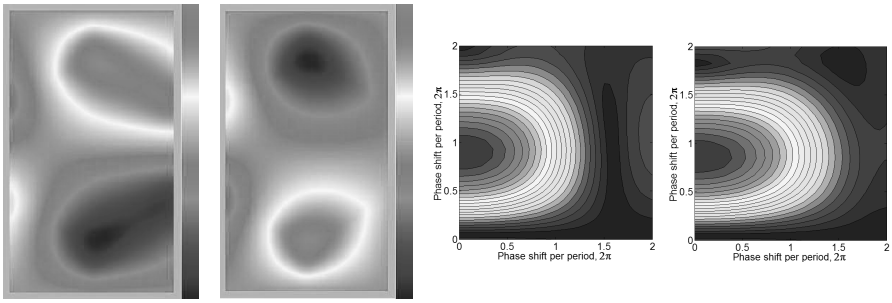


(a) (b) (c) (d)

**Figure 5.** A real part of an electric field amplitude at (a) $f = 102100\,\mathrm{GHz}$ and (b) $f = 109700\,\mathrm{GHz}$ computed for $(\psi_x, \psi_y) = (4/9, 0)2\pi$ in a $1 \times 1$ array of the structure shown in Figure 1, and spatial FFTs computed (c) at the first and (d) at the second frequency.

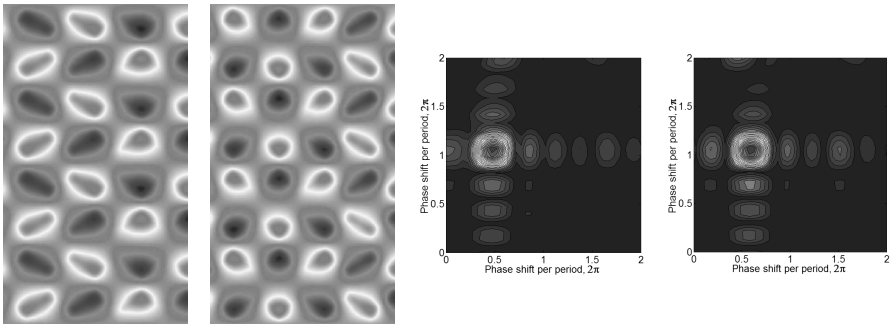


(a) (b) (c) (d)

**Figure 6.** A real part of an electric field amplitude at (a) $f = 102100\,\mathrm{GHz}$ and (b) $f = 109700\,\mathrm{GHz}$ computed for $(\psi_x, \psi_y) = (16/9, 0)2\pi$ in a $4 \times 4$ array of the structure shown in Figure 1, and spatial FFTs computed (c) at the first and (d) at the second frequency.

allowed harmonics of the imposed phase shifts, the nearest solution is found to be $(\psi_x, \psi_y) = (4/9, 1)2\pi$ and $(5/9, 1)2\pi$, respectively. Both points are denoted with **x** and ***** in Figure 2 respectively.

The first mode at $f = 102100\,\mathrm{GHz}$, denoted with **x** in Figure 2, lays on the $\Gamma$-$X_1$ contour but when projected on the hexagonal reciprocal lattice, according to (4), it is located on the $\Gamma$-$K$ contour at $k = 5/6k_K$:

$$\psi_x = \frac{4}{9}2\pi = 2\pi - \frac{5}{9}2\pi = 2\pi - \frac{10}{9}k_{X1}a = 2\pi - \frac{5}{6}k_K a \qquad (6)$$

The second mode at $f = 109700\,\mathrm{GHz}$, denoted with ***** in Figure 2

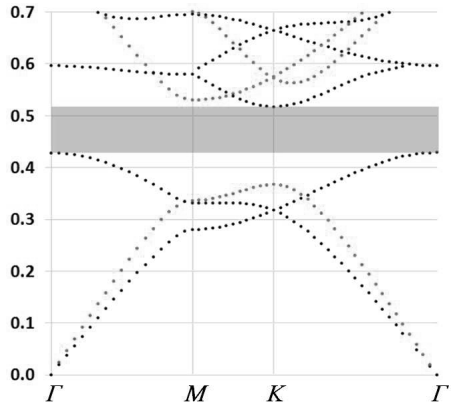


**Figure 7.** A photonic bandgap diagram of the 2D hexagonal lattice shown in Figure 1, computed with the CL-FDTD method and unfolded with the procedure depicted in Figure 3.

at the $(2\pi - \psi_x, 2\pi)$ contour, seems to fall beyond the contours allowed for the imposed set of Floquet phase shifts. However, since FFT is symmetrical with respect to the origin, the solution can also be searched on the opposite side of the 0-$k_y$ axis. Thus, the allowed mode is found on the $(-2\pi + \psi_x, 2\pi)$ contour, as indicated with **o** in Figure 2, while the projection on the hexagonal reciprocal lattice brings it to the $\Gamma$-$K$ contour at $k = 4/6k_K$:

$$\psi_x = -2\pi + \frac{5}{9}2\pi = -\frac{4}{9}2\pi = -\frac{8}{9}k_{X1}a = -\frac{4}{6}k_K a \tag{7}$$

The already presented unfolding process can be easily automated since the relation between rectangular and hexagonal reciprocal lattices, as shown in Figure 2, is explicitly known. Consequently, Figure 7 shows a photonic bandgap diagram of the hexagonal lattice shown in Figure 1 computed with the CL-FDTD method [18, 25] and automatically unfolded with the procedure depicted in Figure 3. The diagram consists of 56 wave vector points. Assuming that each wave vector point requires two CL-FDTD simulations, that is, first to retrieve modal frequencies and, second to compute their field distributions, $56 \times 2 = 112$ simulations have to be carried out. Thus, the total computation time takes 672 seconds, if a single CL-FDTD simulation takes 6 seconds, as it has already been pointed out in this paper. That time does not take into account computational effort of the unfolding procedure but its contribution is usually negligible when compared with the FDTD simulations.

The PBG diagram shown in Figure 7 computed with CL-FDTD is in good agreement with the reference one [1], computed by preconditioned conjugate-gradient minimization of the block Rayleigh quotient in a planewave basis [27] so its plot is omitted here. It successfully validates the unfolding procedure proposed in this paper. It should be emphasized that, in principle, the unfolding procedure does not contribute to the inaccuracy of the PBG diagram computation. The procedure is applicable to detect the modes' position in a wave vector space and to snap them to the nearest allowed spatial harmonics within an irreducible reciprocal lattice followed from the imposed Floquet phase shifts per period $(\psi x, \psi_y)$. Nevertheless, as it has been pointed out in this paper, it can happen that due to low resolution of a spatial FFT the position of the mode will be erroneously evaluated. In such a case, enlargement of the model will solve the issue.

## 4. CONCLUSION

The author has introduced a robust method applicable to the FDTD computation of unfolded PBG diagrams of hexagonal photonic crystals. Unlike alternative solutions, the method proposed in this paper does not require modifications of either an FDTD algorithm or the geometry of the hexagonal lattice. The only cost is in doubled computational effort, since two FDTD simulations have to be carried out per each wave vector point. The first simulation is run to collect resonant frequencies, while the second one is executed to compute modal field distributions at those frequencies. It allows evaluating spatial Fourier transforms determining the position of those modes in the reciprocal lattice.

The author also shows that the contours of a hexagonal Brillouin zone are completely covered, if the calculations are carried out along $\Gamma$-$X_1$ and $\Gamma$-$X_2$ contours of the rectangular counterpart. Although the author focuses in this paper on the hexagonal photonic crystals, the method can be applied to any other non-rectangular lattice type.

## ACKNOWLEDGMENT

Part of this work was funded by the Faculty of Electronics and Information Technology, Warsaw University of Technology, under internal grant No. 504M 1034 4099.

## REFERENCES


1. Joannopoulos, J. D., S. G. Johnson, J. N. Winn, and R. D. Meade, *Photonic Crystals. Molding the Flow of Light*, 2nd Edition, Princeton University Press, 2008.
2. Mekis, A., J. C. Chen, I. Kurland, S. Fan, P. R. Villeneuve, and J. D. Joannopoulos, "High transmission through sharp bends in photonic crystal waveguides," *Physical Review Letters*, Vol. 77, No. 18, 3787–3790, 1996.
3. Yamamoto, N., Y. Watanabe, and K. Komori, "Design of photonic crystal directional coupler with high extinction ratio and small coupling length," *Jpn. J. Appl. Phys.*, Vol. 44, No. 4B, 2575–2578, 2005.
4. Shen, L.-P., W.-P. Huang, and S.-S. Jian, "Design of photonic crystal fibers for dispersion-related applications," *IEEE/OSA J. Lightwave Technol.*, Vol. 21, No. 7, 1644–1651, 2003.
5. Fan, S., P. R. Villeneuve, and J. D. Joannopoulos, "Channel drop filters in photonic crystals," *Optics Letters*, Vol. 3, No. 1, 4–11, 1998.
6. Lu, L., A. Mock, T. Yang, M. H. Shih, E. H. Hwang, M. Bagheri, A. Stapleton, S. Farrell, J. O'Brien, and P. D. Dapkus, "120 μW peak output power from edge-emitting photonic crystal doubleheterostructure nanocavity lasers," *Appl. Phys. Lett.*, Vol. 94, 111101, 2009.
7. Salski, B., "Application of semi-analytical algorithms in the finite-difference time-domain modeling of electromagnetic radiation and scattering problems," Ph.D. Thesis, Warsaw University of Technology, 2010.
8. Collin, R. E., *Field Theory of Guided Waves*, McGraw-Hill Inc., New York, 1960.
9. Liu, L. and J. T. Liu, "Photonic band structure in the nearly plane wave approximation," *Eur. Phys. J. B*, Vol. 9, 381–388, 1999.
10. Johnson, S. G. and J. D. Joannopoulos, "Block-iterative frequency-domain methods for Maxwell's equations in a planewave basis," *Optics Express*, Vol. 8, No. 3, 173–190, 2001.
11. Axmann, W. and P. Kuchment, "An efficient finite element method for computing spectra of photonic and acoustic band-gap materials — I. Scalar case," *J. Comput. Phys.*, Vol. 150, 468–481, 1999.
12. Guo, S., F. Wu, S. Albin, and R. S. Rogowski, "Photonic band gap analysis using finite-difference frequency-domain method," *Optics Express*, Vol. 12, No. 8, 1741–1746, 2004.

13. Taflove, A. and S. C. Hagness, *Computational Electrodynamics — The Finite-difference Time-domain Method*, Artech House, Boston, London, 2005.
14. Gwarek, W. K., "Analysis of an arbitrarily-shaped planar circuit — A time-domain approach," *IEEE Trans. Microw. Theory Tech.*, Vol. 33, No. 10, 1067–1072, 1985.
15. Krietenstein, B., R. Schuhmann, P. Thoma, and T. Weiland, "The perfect boundary approximation technique facing the big challenge of high precision field computation," *19th International Linear Accelerator Conference*, 860–862, 1998.
16. Salski, B., K. Lesniewska-Matys, and P. Szczepanski, "On the applicability of photonic crystal membranes to multi-channel propagation," *Photonic Crystals — Innovative Systems, Lasers and Waveguides*, Chapter 7, InTech, 2012.
17. Loncar, M., B. G. Lee, L. Diehl, M. Belkin, and F. Capasso, "Design and fabrication of photonic crystal quantum cascade lasers for optofluidics," *Optics Express*, Vol. 15, No. 8, 4499–4514, 2007.
18. Celuch-Marcysiak, M. and W. K. Gwarek, "Spatially looped algorithms for time-domain analysis of periodic structures," *IEEE Trans. Microw. Theory Tech*, Vol. 43, No. 4, 860–865, 1995.
19. Ko, W. L. and R. Mittra, "Implementation of Floquet boundary condition in FDTD for FSS analysis," *IEEE APS Int. Symp. Dig.*, Vol. 1, 14–17, 1993.
20. Holland, R., "Finite-difference solution of Maxwell's equations in generalized nonorthogonal coordinates," *IEEE Trans. Nucl. Sci.*, Vol. 30, No. 6, 4589–4591, 1983.
21. Qiu, M. and S. He, "A nonorthogonal finite-difference time-domain method for computing the band structure of a two-dimensional photonic crystal with dielectric and metallic inclusions," *Appl. Phys.*, Vol. 87, 8268–8275, 1992.
22. Yu, C. and H. Chang, "Compact finite-difference frequency-domain method for the analysis of two-dimensional photonic crystals," *Optics Express*, Vol. 12, No. 7, 1397–1408, 2004.
23. Ma, Z. and K. Ogusu, "FDTD analysis of 2D triangular-lattice photonic crystals with arbitrary-shape inclusions based on unit cell transformation," *Optics Communications*, Vol. 282, 1322–1325, 2009.
24. Kuang, W., W. J. Kim, and J. D. O'Brien, "Finite-difference time domain method for nonorthogonal unit-cell two-dimensional photonic crystals," *J. Lightw. Technol.*, Vol. 25, No. 9, 2612–2617,

2007.

25. Gwarek, W., M. Celuch, A. Wieckowski, and M. Sypniewski, *QuickWave User Manuals*, Warsaw, 1997–2012, www.qwed.eu.
26. Salski, B., M. Celuch, and W. K. Gwarek, "Review of Complex Looped FDTD and its new applications," *24th Annual Review of Progress in Applied Computational Electromagnetics*, Niagara, Falls, 2008.
27. Johnson, S. G. and J. D. Joannopoulos, "Block-iterative frequency-domain methods for Maxwell's equations in a planewave basis," *Optics Express*, Vol. 8, No. 3, 173–190, 2001.